JACS
JOURNAL OF THE AMERICAN CHEMICAL SOCIETY
Communication
pubs.acs.org/JACS

$La_{0.8}Sr_{0.2}MnO_{3-\delta}$ Decorated with $Ba_{0.5}Sr_{0.5}Co_{0.8}Fe_{0.2}O_{3-\delta}$: A Bifunctional Surface for Oxygen Electrocatalysis with Enhanced Stability and Activity

Marcel Risch,[†] Kelsey A. Stoerzinger,[‡] Shingo Maruyama,[§,⊥] Wesley T. Hong,[‡] Ichiro Takeuchi,[§] and Yang Shao-Horn*[,†,‡,∥]

[†]Research Laboratory of Electronics, Massachusetts Institute of Technology, Cambridge, Massachusetts 02139, United States
[‡]Department of Materials Science and Engineering, Massachusetts Institute of Technology, Cambridge, Massachusetts 02139, United States
[§]Department of Materials Science and Engineering, University of Maryland, College Park, Maryland 20742, United States
[∥]Department of Mechanical Engineering, Massachusetts Institute of Technology, Cambridge, Massachusetts 02139, United States

Supporting Information

ABSTRACT: Developing highly active and stable catalysts based on earth-abundant elements for oxygen electrocatalysis is critical to enable efficient energy storage and conversion. In this work, we took advantage of the high intrinsic oxygen reduction reaction (ORR) activity of $La_{0.8}Sr_{0.2}MnO_{3-\delta}$ (LSMO) and the high intrinsic oxygen evolution reaction (OER) activity of $Ba_{0.5}Sr_{0.5}Co_{0.8}Fe_{0.2}O_{3-\delta}$ (BSCF) to develop a novel bifunctional catalyst. We used pulsed laser deposition to fabricate well-defined surfaces composed of BSCF on thin-film LSMO grown on (001)-oriented Nb-doped $SrTiO_3$. These surfaces exhibit bifunctionality for oxygen electrocatalysis with enhanced activities and stability for both the ORR and OER that rival the state-of-the-art single- and multicomponent catalysts in the literature.

Oxygen electrocatalysis is central to the development of efficient energy storage and conversion devices[1] such as metal−air batteries[2] and regenerative fuel cells[3] to link intermittent renewable energy with energy needs on-demand. Progress is hampered by the large intrinsic overpotentials of the oxygen reduction reaction (ORR)[1d,4] and oxygen evolution reaction (OER) kinetics,[5] particularly for first-row transition metal oxides as cost-effective alternatives to catalysts containing Pt, Ru, or Ir.[1c,5c,f−i,6] An equally important challenge is the stability of catalysts during oxygen electrocatalysis.[4a,5a,7] In our previous work,[4d,5f] we have systematically studied the ORR and OER activities per oxide area (intrinsic activities) of first-row transition metal-based perovskites, as measured by the overpotential at 50 $\mu A/cm_{ox}^2$.

Perovskites can have intrinsic activities comparable to those of precious-metal-based catalysts, and we have used activity descriptors based on the electronic structure of perovskites to identify new oxide chemistries with enhanced activities.[4d,5f,6,8] Manganite perovskites were among the most active for ORR in our previous studies of perovskite oxides[4d,9] but have low intrinsic activity for OER, while $Ba_{0.5}Sr_{0.5}Co_{0.8}Fe_{0.2}O_{3-\delta}$ (BSCF) exhibited the highest intrinsic activity for OER among perovskites and rutile IrO_2 but lower intrinsic activity for ORR.[4d,5f,9,10] In this study, we fabricated BSCF-decorated (001)-oriented $La_{0.8}Sr_{0.2}MnO_{3-\delta}$ (LSMO) surfaces (where all orientations herein refer to the pseudocubic unit cell), and here we report their bifunctionality for oxygen electrocatalysis with intrinsic ORR and OER activities rivaling the most active catalysts in the literature.

Thin films with the (001) orientation were fabricated in a two-step process. First, a ∼16 nm layer of LSMO was grown by pulsed laser deposition (PLD) on a 0.5 wt % Nb-doped $SrTiO_3$ (NSTO) substrate with (001) orientation. Second, BSCF layers with target thicknesses of 1, 2, 5, 10, and 20 nm were deposited onto LSMO by PLD. We denote these films as BSCF|LSMO|NSTO. More experimental details can be found in the Supporting Information (SI). The use of well-defined thin films reduces the uncertainty of oxide surface area estimation and the influence of different crystallographic orientations on the activity relative to oxide powder.[9] In addition, these thin films exclude carbon additives often used in the measurement of oxide powders, eliminating the reasonably high ORR current contribution from carbon.[9,11] After fabrication, the BSCF|LSMO|NSTO thin films were characterized by X-ray diffraction (XRD) (Figure S1 and Table S1), Raman spectroscopy (Figure S2), X-ray reflectivity (XRR) (Figure S3 and Table S1), and atomic force microscopy (AFM) (Figure 1) to elucidate the crystal structure, distortion of the local structure, layer thicknesses, and surface morphology, respectively. The (002) Bragg peaks of the BSCF thin films were observable by XRD at greater thicknesses (19.3, 7.9, and 3.8 nm), which indicates epitaxy for these films, and the observed lattice parameters were in agreement with that of bulk BSCF powder (space group $Pm\bar{3}m$; Table S1). Moreover, the Raman spectra of these films show features similar to those of BSCF powder (Figure S2),[10a,12] indicating local symmetry comparable to the bulk.[10a,12] Furthermore, island growth of BSCF on LSMO is evident from AFM (Figure 1), and the coverage of BSCF on LSMO was found to increase from 20% to 94% for thicknesses

Received: January 28, 2014
Published: March 20, 2014

   dx.doi.org/10.1021/ja5009954 | J. Am. Chem. Soc. 2014, 136, 5229−5232

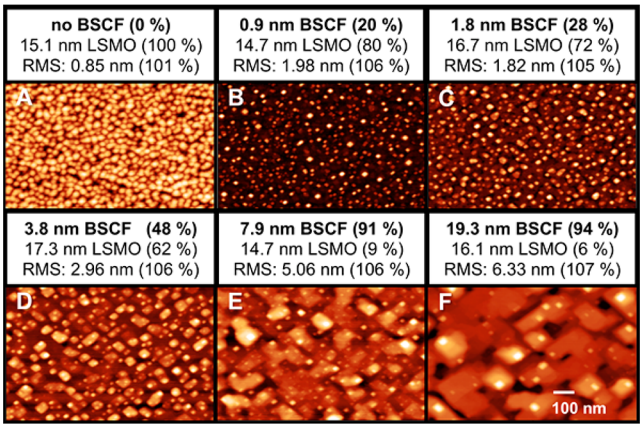

Figure 1. Surface morphology of BSCF|LSMO|NSTO thin films obtained by AFM in tapping mode. The surface coverage of BSCF (percentage in parentheses) was estimated from the projected area of the grains (yellow). It should be noted that the color scale differs for each sample. The percentage given after the root-mean-square (RMS) roughness indicates the roughness factor (calculated total surface area divided by scan area).

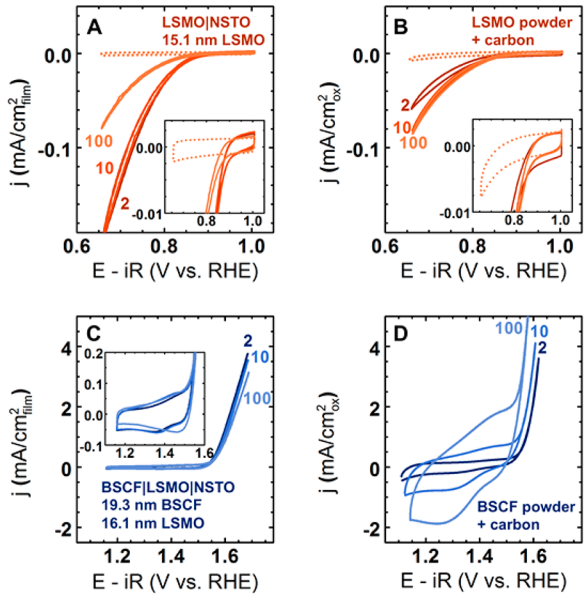

Figure 2. Cyclic voltammetry of (A) an LSMO|NSTO thin film in comparison with (B) ink-cast LSMO powder and (C) a BSCF|LSMO|NSTO thin film in comparison with (D) ink-cast BSCF powder.[10a] The 2nd, 10th, and 100th cycles in O_2-purged 0.1 M at sweep speed of 10 mV/s are shown as solid lines. Dashed lines indicate measurements in Ar-purged 0.1 M KOH.. The ink-cast electrodes had loadings of 0.25 mg/cm_{disk}^2 for oxide, 0.05 mg/cm_{disk}^2 for carbon, and 0.05 mg/cm_{disk}^2 for Nafion. Currents were normalized by the BET areas (Table S3) for ink-cast oxides and by the measured electrode area and the roughness factor for thin films (Table S2).

of 0.9 to 19.3 nm, respectively. As most of the island radii were much larger than the thickness (Figure S4), the influence of different crystallographic orientations associated with island edges on the activity can be neglected. All of the electrochemical measurements were corrected for the roughness factor of the thin films (see the SI for the calculations).

The activity and stability trends of the thin films were established by cycling 100 times in the OER region (1.15 to 1.70 V vs RHE) and subsequently 100 times in the ORR region (1.00 to 0.65 V vs RHE) in 0.1 M KOH (pH 13). Alkaline conditions are preferable for testing of intrinsic activities because of the excellent oxide stability and fast kinetics of the OER and ORR at pH 13. The intrinsic ORR activity of LSMO|NSTO (Figure 2A) in the first few cycles was among the highest reported (10 μA/cm_{film}^2 at 0.85 V vs RHE/0.38 V overpotential),[4d] which is comparable to those of LSMO powder (Figure 2B) and previously reported[4d] $LaMnO_3$ (LMO) and $La_{0.5}Ca_{0.5}MnO_{3-\delta}$ powders. This finding suggests that the (001) perovskite surface is primarily responsible for the ORR activity of LSMO, which is in agreement with previous work on LMO thin films.[9] However, the ORR activity of LSMO|NSTO decreased during cycling (Figure 2A), which will be discussed in detail later. In contrast, the intrinsic OER activity of LSMO|NSTO was among the lowest of perovskite oxides (23 μA/cm_{film}^2 at 1.56 V vs RHE/0.33 V overpotential) and comparable to that of LSMO powder[5f,13] (Figure S5). On the other hand, the intrinsic OER activity of BSCF|LSMO|NSTO (nearly full coverage of BSCF of ~94%) was found to be among the highest reported for perovskite oxides (0.5 mA/cm_{film}^2 at 1.56 V vs RHE/0.33 V overpotential) and comparable to that of pristine BSCF powder[5f,10a,14] within experimental uncertainties (Figure S6).

No significant change was found for the OER activities and pseudocapacitive current densities of the BSCF|LSMO|NSTO films (Figure 2C) during cycling, in contrast to BSCF powder (Figure 2D).[10a] The increase in the OER current and pseudocapacitive current of BSCF powder during cycling in the OER voltage region has been attributed to an increase in the electrochemically active area associated with leaching of Ba and Sr ions, loss of long-range order, and a change of the local structure from corner-sharing to edge-sharing octahedra, as reported previously.[10] The cyclic voltammogram (CV) of BSCF|LSMO|NSTO after 100 OER cycles resembles that of a hydroxide,[10b] indicating similar changes of (001)-oriented BSCF on LSMO to BSCF powder, which requires further studies. This hypothesis is further supported by the scaling of the OER current with cathodic charge for BSCF coverage equal to and lower than 48% (Figure S7). Therefore, not only the film surface but also BSCF away from the film surface on LSMO contributes to the OER activity, akin to amorphous oxyhydroxides.[15] Interestingly, the measured cathodic charge corresponded to a reduction of up to 77% of all transition metal ions nominally present in the thinnest films (Table S4). Even the lowest value of 24% (for 94% BSCF coverage) rivals the values reported for electrodeposited oxides.[15b,c]

Partially BSCF-covered LSMO surfaces (20−91%) were found to have not only high activities for both OER and ORR but also enhanced stability for ORR relative to LSMO (Figure 3). The intrinsic OER activity could be increased by 2 orders of magnitude relative to LSMO|NSTO by increasing the BSCF coverage (Figure 3A−C), where negligible change in the OER activity was found during cycling. The Tafel slopes for the OER activities of all BSCF|LSMO|NSTO samples were similar (~50 mV/dec) and independent of BSCF coverage (Figure 3B) as well as the method of measurement (Figure S9), which is comparable to BSCF powder (Figure S10). On the other hand, the ORR activities of BSCF|LSMO|NSTO with BSCF coverage less than 94% were greater than or comparable to that of pristine LSMO|NSTO (Figure 3D−F). The ORR Tafel slopes extracted from low overpotentials, where the influence of oxygen transport is minimal, were similar and close to 50 mV/dec for all of the surfaces studied (Figure 3E), which

dx.doi.org/10.1021/ja5009954 | J. Am. Chem. Soc. 2014, 136, 5229−5232

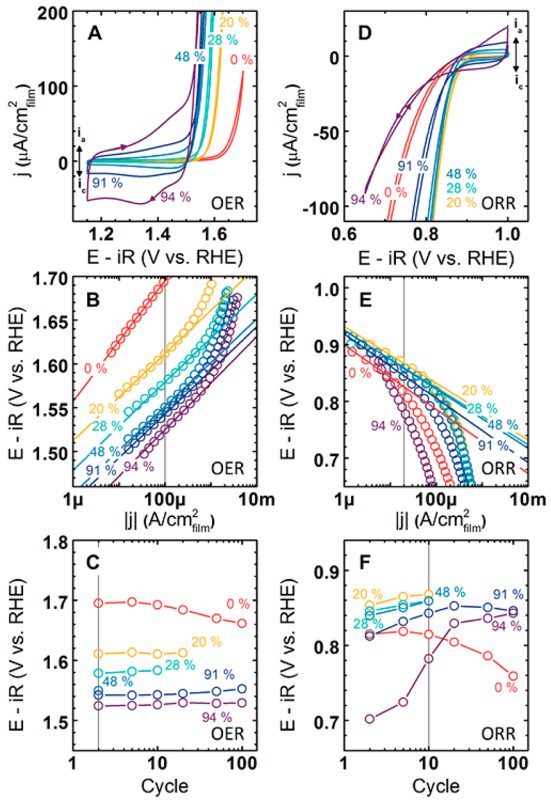

Figure 3. (A) CVs of BSCF|LSMO|NSTO thin films in the OER window during the 2nd cycle, (B) Tafel plot of the capacitance-corrected CV (Figure S8), and (C) change in the potential at 100 $\mu A/cm_{film}^2$ OER current density with cycling. (D) Subsequent CVs of the same films in the ORR window during the 10th cycle, (E) Tafel plot of the capacitance-corrected background-subtracted CV, and (F) change in the potential at 20 $\mu A/cm_{film}^2$ ORR current density with cycling. All of the measurements were performed at a sweep speed of 10 mV/s in 0.1 M KOH purged with O_2. For the ORR Tafel plot, the background currents obtained in Ar-purged 0.1 M KOH were subtracted. Percentages indicate BSCF coverage. All of the currents were normalized by the measured electrode area and the roughness factor (Table S1).

is comparable to LMSO|NSTO (Figure S10). These observations suggest that BSCF|LSMO|NSTO surfaces with partial coverage exhibit bifunctional catalytic properties, where BSCF is responsible for the OER activity while LSMO is responsible for the ORR activity. More interestingly, while cycling in the ORR region did not alter the OER activity of BSCF|LSMO|NSTO, it greatly increased the ORR activity of films with greater BSCF coverage to be higher than that of pristine LSMO|NSTO (Figures 3F and S11). This stands in contrast to the reduced ORR activity of LSMO|NSTO during cycling. The physical origin for these changes is not understood and warrants further studies. The OER activity of LSMO|NSTO was increased slightly during OER cycling (Figure S12), which can be attributed to gradual manganese oxidation and structural changes during OER akin to those observed for amorphous manganese oxyhydroxide.[15a] Manganese oxidation during the OER is supported by the decreased activity for subsequent ORR measurements (Figure 3D), as we have demonstrated previously that Mn^{3+} is more active for the ORR than Mn^{4+}.[9]

The intrinsic OER and ORR activities of BSCF|LSMO|NSTO are among the highest for bifunctional catalysts known in the literature (Figure 4A); the intrinsic OER activity

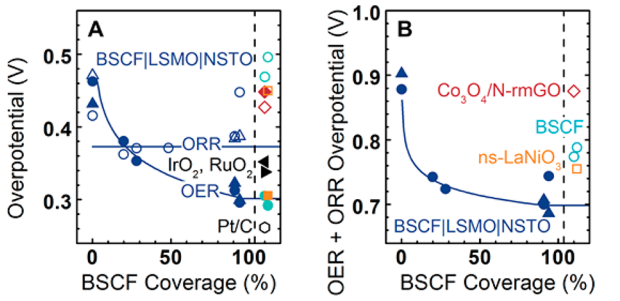

Figure 4. (A) OER and ORR overpotentials of BSCF|LSMO|NSTO electrodes at 100 $\mu A/cm_{film}^2$ OER current density (solid circles) and 20 $\mu A/cm_{film}^2$ ORR current density at the 10th cycle (open circles) and 100th cycle (triangles) in 0.1 M KOH. For reference, we have also included the overpotentials of selected bifunctional oxides[5f,14,16] (Figures S6 and S13–S15) at the above current densities and benchmarks for intrinsic OER (IrO_2, RuO_2)[5e] and ORR (Pt/C)[14] activities. (B) Sum of OER and ORR overpotentials. Lines were added to guide the eye.

surpasses those of the benchmark catalysts, IrO_2 and RuO_2,[5e] and the intrinsic ORR activity is superior to those of other bifunctional oxides, albeit lower than that of Pt/C,[14] the benchmark for the ORR. While the normalization of OER and ORR currents by geometric areas is most relevant for practical applications, such as overpotentials for the OER at 10 mA/cm_{geo}^2 and ORR at 3 mA/cm_{geo}^2 current density,[17] the overpotential for a given OER or ORR specific current (normalized to the oxide surface area) allows us to compare the intrinsic activities of surfaces. Here we used the OER current density at 100 $\mu A/cm_{ox}^2$ and absolute ORR current density at 20 $\mu A/cm_{ox}^2$ (Figure 4A), which were chosen to avoid mass transport limitations in experiments with quiescent electrolytes and to minimize the influence of pseudocapacitive contributions. The lowest combined overpotential for OER and ORR approaches 0.7 V for BSCF|LSMO|NSTO thin films with nearly full BSCF coverage (Figure 4B), which rivals the intrinsic bifunctional activities of state-of-the-art single- and multi-component oxide catalysts reported in the literature.[5f,16]

In this work, we have shown that BSCF decoration on LSMO|NSTO comprises a two-component surface with bifunctionality for oxygen electrocatalysis, with OER activities comparable to that of BSCF powder and ORR activities surpassing that of LSMO powder. The combined overpotentials from both OER and ORR kinetics on BSCF|LSMO|NSTO can be as low as 0.7 V, which rivals the intrinsic activities of state-of-the-art catalysts in the literature. Moreover, BSCF decoration enhances the surface stability for the ORR relative to LSMO|NSTO, although this requires further studies. Such work lends promising insights into the design of highly active and stable nanostructured bifunctional catalysts for oxygen electrocatalysis in rechargeable metal–air batteries and regenerative fuel cells.

■ ASSOCIATED CONTENT

Ⓢ Supporting Information

Experimental details, additional electrochemical data, XRD and XRR patterns, and Raman spectra. This material is available free of charge via the Internet at http://pubs.acs.org.

■ AUTHOR INFORMATION

Corresponding Author

shaohorn@mit.edu

dx.doi.org/10.1021/ja5009954 | J. Am. Chem. Soc. 2014, 136, 5229–5232

Present Address

[⊥]S.M.: Department of Applied Chemistry, Graduate School of Engineering, Tohoku University, Sendai 980-8579, Japan.

Notes

The authors declare no competing financial interest.

■ ACKNOWLEDGMENTS

This work was supported in part by the DOE Hydrogen Initiative Program under Award DE-FG02-05ER15728 and the MRSEC Program of the National Science Foundation under Award DMR-0819762. K.A.S. was supported by a National Science Foundation Graduate Research Fellowship (Grant DGE-1122374).

■ REFERENCES

(1) (a) Lewis, N. S.; Nocera, D. G. *Proc. Natl. Acad. Sci. U.S.A.* **2006**, *103*, 15729. (b) Gray, H. B. *Nat. Chem.* **2009**, *1*, 7. (c) Dau, H.; Limberg, C.; Reier, T.; Risch, M.; Roggan, S.; Strasser, P. *ChemCatChem* **2010**, *2*, 724. (d) Nørskov, J. K.; Rossmeisl, J.; Logadottir, A.; Lindqvist, L.; Kitchin, J. R.; Bligaard, T.; Jónsson, H. *J. Phys. Chem. B* **2004**, *108*, 17886. (e) Pinaud, B. A.; Benck, J. D.; Seitz, L. C.; Forman, A. J.; Chen, Z.; Deutsch, T. G.; James, B. D.; Baum, K. N.; Baum, G. N.; Ardo, S.; Wang, H.; Miller, E.; Jaramillo, T. F. *Energy Environ. Sci.* **2013**, *6*, 1983. (f) Service, R. F. *Science* **2009**, *324*, 1257. (g) Greeley, J.; Stephens, I. E. L.; Bondarenko, A. S.; Johansson, T. P.; Hansen, H. A.; Jaramillo, T. F.; Rossmeisl, J.; Chorkendorff, I.; Nørskov, J. K. *Nat. Chem.* **2009**, *1*, 552. (h) Kinoshita, K. E. S. *Electrochemical Oxygen Technology*; Wiley: New York, 1992.

(2) (a) Park, M.; Sun, H.; Lee, H.; Lee, J.; Cho, J. *Adv. Energy Mater.* **2012**, *2*, 780. (b) Cao, R.; Lee, J.-S.; Liu, M.; Cho, J. *Adv. Energy Mater.* **2012**, *2*, 816.

(3) (a) Mitlitsky, F.; Myers, B.; Weisberg, A. H. *Energy Fuels* **1998**, *12*, 56. (b) Desmond Ng, J. W.; Gorlin, Y.; Hatsukade, T.; Jaramillo, T. F. *Adv. Energy Mater.* **2013**, *3*, 1545.

(4) (a) Gasteiger, H. A.; Kocha, S. S.; Sompalli, B.; Wagner, F. T. *Appl. Catal., B* **2005**, *56*, 9. (b) McGuire, R., Jr.; Dogutan, D. K.; Teets, T. S.; Suntivich, J.; Shao-Horn, Y.; Nocera, D. G. *Chem. Sci.* **2010**, *1*, 411. (c) Stamenkovic, V. R.; Mun, B. S.; Arenz, M.; Mayrhofer, K. J. J.; Lucas, C. A.; Wang, G.; Ross, P. N.; Markovic, N. M. *Nat. Mater.* **2007**, *6*, 241. (d) Suntivich, J.; Gasteiger, H. A.; Yabuuchi, N.; Nakanishi, H.; Goodenough, J. B.; Shao-Horn, Y. *Nat. Chem.* **2011**, *3*, 546.

(5) (a) McCrory, C. C. L.; Jung, S.; Peters, J. C.; Jaramillo, T. F. *J. Am. Chem. Soc.* **2013**, *135*, 16977. (b) Rossmeisl, J.; Qu, Z. W.; Zhu, H.; Kroes, G. J.; Nørskov, J. K. *J. Electroanal. Chem.* **2007**, *607*, 83. (c) Man, I. C.; Su, H.-Y.; Calle-Vallejo, F.; Hansen, H. A.; Martínez, J. I.; Inoglu, N. G.; Kitchin, J.; Jaramillo, T. F.; Nørskov, J. K.; Rossmeisl, J. *ChemCatChem* **2011**, *3*, 1159. (d) Risch, M.; Suntivich, J.; Shao-Horn, Y. In *Encyclopedia of Applied Electrochemistry: SpringerReference*; Savinell, R., Ota, K., Kreysa, G., Eds.; Springer: Berlin, 2013; DOI: 10.1007/SpringerReference_303858. (e) Lee, Y.; Suntivich, J.; May, K. J.; Perry, E. E.; Shao-Horn, Y. *J. Phys. Chem. Lett.* **2012**, *3*, 399. (f) Suntivich, J.; May, K. J.; Gasteiger, H. A.; Goodenough, J. B.; Shao-Horn, Y. *Science* **2011**, *334*, 1383. (g) Bockris, J. O. M.; Otagawa, T. *J. Electrochem. Soc.* **1984**, *131*, 290. (h) Trasatti, S. *J. Electroanal. Chem.* **1980**, *111*, 125. (i) Kanan, D. K.; Keith, J. A.; Carter, E. A. *ChemElectroChem* **2014**, *1*, 407.

(6) Grimaud, A.; May, K. J.; Carlton, C. E.; Lee, Y.-L.; Risch, M.; Hong, W. T.; Zhou, J.; Shao-Horn, Y. *Nat. Commun.* **2013**, *4*, 2439.

(7) Ferreira, P. J.; la O', G. J.; Shao-Horn, Y.; Morgan, D.; Makharia, R.; Kocha, S.; Gasteiger, H. A. *J. Electrochem. Soc.* **2005**, *152*, A2256.

(8) Lee, Y.-L.; Kleis, J.; Rossmeisl, J.; Shao-Horn, Y.; Morgan, D. *Energy Environ. Sci.* **2011**, *4*, 3966.

(9) Stoerzinger, K. A.; Risch, M.; Suntivich, J.; Lü, W. M.; Zhou, J.; Biegalski, M. D.; Christen, H. M.; Ariando; Venkatesan, T.; Shao-Horn, Y. *Energy Environ. Sci.* **2013**, *6*, 1582.

(10) (a) May, K. J.; Carlton, C. E.; Stoerzinger, K. A.; Risch, M.; Suntivich, J.; Lee, Y.-L.; Grimaud, A.; Shao-Horn, Y. *J. Phys. Chem. Lett.* **2012**, *3*, 3264. (b) Risch, M.; Grimaud, A.; May, K. J.; Stoerzinger, K. A.; Chen, T. J.; Mansour, A. N.; Shao-Horn, Y. *J. Phys. Chem. C* **2013**, *117*, 8628.

(11) Malkhandi, S.; Trinh, P.; Manohar, A. K.; Jayachandrababu, K. C.; Kindler, A.; Surya Prakash, G. K.; Narayanan, S. R. *J. Electrochem. Soc.* **2013**, *160*, F943.

(12) Gangopadhayay, S.; Inerbaev, T.; Masunov, A. m. E.; Altilio, D.; Orlovskaya, N. *ACS Appl. Mater. Interfaces* **2009**, *1*, 1512.

(13) Grimaud, A.; Carlton, C. E.; Risch, M.; Hong, W. T.; May, K. J.; Shao-Horn, Y. *J. Am. Chem. Soc.* **2013**, *117*, 25926.

(14) Suntivich, J.; Perry, E.; Gasteiger, H.; Shao-Horn, Y. *Electrocatalysis* **2013**, *4*, 49.

(15) (a) Gorlin, Y.; Lassalle-Kaiser, B.; Benck, J. D.; Gul, S.; Webb, S. M.; Yachandra, V. K.; Yano, J.; Jaramillo, T. F. *J. Am. Chem. Soc.* **2013**, *135*, 8525. (b) Risch, M.; Klingan, K.; Ringleb, F.; Chernev, P.; Zaharieva, I.; Fischer, A.; Dau, H. *ChemSusChem* **2012**, *5*, 542. (c) Klingan, K.; Ringleb, F.; Zaharieva, I.; Heidkamp, J.; Chernev, P.; Gonzalez-Flores, D.; Risch, M.; Fischer, A.; Dau, H. *ChemSusChem* **2014**, DOI: 10.1002/cssc.201301019.

(16) (a) Liang, Y.; Li, Y.; Wang, H.; Zhou, J.; Wang, J.; Regier, T.; Dai, H. *Nat. Mater.* **2011**, *10*, 780. (b) Hardin, W. G.; Slanac, D. A.; Wang, X.; Dai, S.; Johnston, K. P.; Stevenson, K. J. *J. Phys. Chem. Lett.* **2013**, *4*, 1254. (c) Jin, C.; Cao, X.; Lu, F.; Yang, Z.; Yang, R. *Int. J. Hydrogen Energy* **2013**, *38*, 10389.

(17) (a) Gorlin, Y.; Jaramillo, T. F. *J. Am. Chem. Soc.* **2010**, *132*, 13612. (b) Weber, M. F.; Dignam, M. J. *J. Electrochem. Soc.* **1984**, *131*, 1258.